Arch bridges subject to pier settlements: continuous vs. piecewise rigid displacement methods

Marialaura Malena · Maurizio Angelillo · Antonio Fortunato · Gianmarco de Felice [ORCID] ·
Ida Mascolo

Abstract Settlements severely affect historic masonry arch bridges worldwide. There are countless examples of structural dislocations and ruins in recent years due to severe settlements at the base of pier foundations, often caused by shipworm infestation of wooden foundations or scouring and riverbed erosion phenomena. The present paper proposes an original way to approach the failure analysis of settled masonry arch bridges. The proposed method combines two different 2D numerical models for the prediction of masonry arch bridge capacity against settlements and for safety assessment. The first one is the Piecewise Rigid Displacement method, i.e. a block-based limit analysis approach using the well known Heyman's hypotheses; the second one is a continuous Finite Element approach. The case study of the four-span Deba Bridge (Spain, 2018) failure is presented with the aim to illustrate how the methods work. The failure analysis produced satisfactory results by applying both methods separately, in confirmation of their reliability. Their combination also allowed to obtain a significantly reduction in computational cost and an improvement of prediction accuracy. A sensitivity and a path-following analysis were also performed with the aim to demonstrate the robustness of the presented method. The obtained simulations highlighted that the results do not depend on the friction angle and that a proper prediction of the evolution of the structural behavior can be obtained only taking into account geometric nonlinearities. Such results demonstrate once again that in settled masonry arches geometry prevails over the mechanical parameters. The current study paves the way for the fruitful use of the proposed approaches for a wider range of applications, as, for example, the mechanism identification or the displacement capacity assessment of masonry structures under overloading as seismic loads.

Keywords Masonry · Arch bridge · Piecewise rigid displacement method · Finite element method

M. Malena · G. de Felice (✉)
Department of Engineering, Roma Tre University, Via Vito Volterra, 62, Rome, RM 00146, Italy
e-mail: defelice@uniroma3.it

M. Malena
e-mail: marialaura.malena@uniroma3.it

M. Angelillo · A. Fortunato · I. Mascolo
Department of Civil Engineering, University of Salerno, via Giovanni Paolo II, 132, Fisciano, SA 84084, Italy
e-mail: mangelillo@unisa.it

A. Fortunato
e-mail: a.fortunato@unisa.it

I. Mascolo
e-mail: i.mascolo@unisa.it

1 Introduction

Masonry arch bridges are widespread throughout Europe and worldwide. They are admirable engineering works with paramount socio-economic value and profile of cultural heritage which quite often are overlooked and underrated. Despite they are characterized by high durability when compared to other types of bridges, there have been several instances of serious structural failure of masonry arch bridges over recent years around the world due to exceptional loading like flood and massive differential settlements (Figs. 1 and 2). This dramatically demonstrates the need of accurate predictions of masonry arch bridge capacity against settlements.

In the last years, intensive research has been carried out to develop numerical models with different degrees of complexity able to describe the non-simple behavior of masonry arches bridges under external loads. All these models follow one of the two main numerical approaches adopted more in general for the numerical analysis of masonry structures: limit analysis-based solutions and path-following analyses.

The first mentioned approach is based on Heyman's hypotheses [1]: masonry has no tensile strength, the compressive strength of masonry is infinite, sliding of one masonry block upon another cannot occur. Firstly,
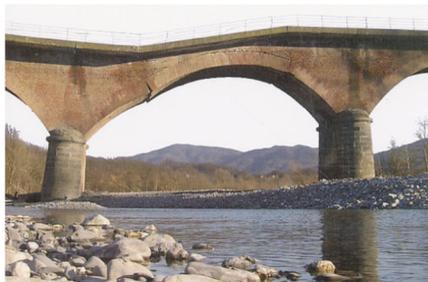
(a) Scrivia river bridge (IT, 2002) Cortesy of Camilla Torre [29]

(b) Trigno (IT, 2003) [10]

(c) Cesano river bridge (IT, 2011) [30]

(d) Rubianello bridge (IT, 2013) [12]

(e) Ballynameen Bridge (UK, 2015) [28].

(f) Bishopsford Road Bridge (UK, 2019)

Fig. 1 Recent worldwide masonry bridge failures under scour-induced settlements

Fig. 2 Deba bridge failure under pier settlement induced by pile shipworm infestation: **a** general view; **b** second pier

these assumptions only allowed analysis of common seismic failure modes of masonry buildings [2], nowadays, they give a solid base for the formulation of modern computational limit analysis-based methods. One of the main disadvantages of limit analysis-based solutions consists in the fact that their output is limited to the collapse multiplier and the collapse mechanism, and no information is available on the ultimate displacement and post-peak response.

In path-following analysis procedures, the evolution of the equilibrium conditions of a structure subjected to certain actions is investigated step-by-step. A peculiarity of these procedures is the possibility to account for mechanical and geometric nonlinearities, which is fundamental and mandatory to be considered for a reliable assessment of the collapse behavior of masonry structures.

Several scientific works are concerned with the study of the load carrying capacity of masonry arch bridges subject to traffic loads [3, 4] or with the assessment under earthquake loading [5–7] and [8] while only a few numerical simulations try to describe the vulnerability of masonry arch bridges to pier's settlements: in [9] , [10–12] path-following analyses carried out on 2D or 3D finite element models of multispan masonry bridges subject to scour induced settlement are presented; in [13, 14] a limit analysis-based numerical solution for masonry arch bridges subject to piers' settlement is proposed.

In the present paper we propose two numerical models for the numerical analysis of masonry arch bridges subject to pier's settlement.

The first one, the Piecewise Rigid Displacement (PRD) method [15–17], is a geometry-based model since the geometry of the structure represents the sole input datum, besides the body loads and the displacement and loading boundary conditions. Working

within the consolidated framework of limit analysis, this method is able to predict the fracture pattern (i.e. the rigid macro-block partition of the structure) by minimizing the Total Potential Energy (TPE) [18].

The second one is a nonlinear finite element model [19, 20]. For which masonry walls are represented as elasto-plastic homogenized solids in 2D plane state, with an associated flow-rule. The model is formulated in the framework of multi-surface plasticity and is implemented in a FE code. The numerical analyses carried out with the above-mentioned model are incremental-iterative analyses, able to follow step-by-step the evolution of the equilibrium conditions of a structure subjected to certain actions: as for the previous method, this method does not require the a priori definition of the collapse mechanism. The method has been adopted for the solution of several problems: soil-structure interaction [21], collapse mechanism analysis of masonry churches [22] and effect of settlements [23].

Here the Authors try to take advantages of these two numerical approaches by combining them in order to propose a simple numerical tool able to realistically describe the mechanical behavior of masonry arch bridges and to prove their structural soundness under pier's settlements. The two above-mentioned approaches are adopted in sequence: first the numerical simulation with the PRD method is carried out to identify the main critical zones in the geometry of the analyzed masonry structure. Then, the definition of the finite element model following the second approach is based on the results of the PRD method: using a coarse mesh in the zones where no cracks are reveled from the PRD model results, and a finer mesh where cracks are predicted by PRD method. A consequence of this choice is the possibility to significantly cut down on

the number of degrees of freedom reducing the computational costs.

The two approaches has been validated by applying them to a case study: the Deba Bridge in Spain. The paper will proceed as follows. Section 2 briefly stresses the role of settlements in masonry arch bridge failures, with a brief overview of high-value masonry arch bridge failures in Europe over the last two decades. Section 3 focuses on the Deba Bridge and its failures over the years, presenting the historical context, the construction details and giving accurate information on its last failure, dating back to 2018. Sections 4 and 5 present the theoretical framework of the proposed numerical approach and its application to the presented case study. The findings have been confronted and validated by a comparison with the geometrical survey of the Deba bridge failure and an in-depth discussion is also provided. The comparison has revealed a good agreement between the numerical-based fracture pattern and the observed one. This highlights the consistency and robustness of the proposed method, as it is emphasized in the concluding remarks drawn in Sect. 6.

2 Effects of settlements on masonry arch bridges

Among the most common causes which can induce settlements at the base of pier foundations are the shipworm infestation of wooden foundations and the scouring and riverbed erosion phenomena [24, 25].

Shipworms (i.e. wood-boring organisms) infestation on underwater timber foundation can develop pole weakness (i.e. severe loss of section, deterioration and decrease of mechanical properties etc.) leading to sudden foundation settlements. Similarly local scouring induced by turbulence and vortex shedding close to bridge piers and riverbed erosion phenomena cause undermining of foundations or extensive settlements at the base of pier foundations. This is even more true when the bridge rests on shallow foundations. Either case results in severe distortions producing a significant load carrying capacity reduction, performance losses, damage and in extreme conditions the structural collapse of the bridge.

Past and recent history is full of tragic examples of masonry arch bridges failures under scour-induced settlements, especially as a result of hazardous events

such as flood. Nevertheless, the problem is not still properly treated in the pertinent literature [10–12].

During Storm Desmond in 2015, for example, about 650 bridges in UK were damaged in the floods. The County of Cumbria, in North East England was the area most affected [26]. Historic masonry arch Brougham Old Bridge over the River Eamont, near Penrith (UK), was one of the bridges damaged in the floods. This bridge suffered significant damage under scour-induced settlements [27] leading to its closure for two years. An other well known case, is the Ballynameen Bridge [28], an arch masonry bridge over the River Faughn near Cladys, Northern Ireland, that partially collapsed due to a scour at the front of the central pier.

But there are many further noticeable examples throughout the world. In England (on June 14th 2019), for example, jack post installations caused scour at the northern arch pier of Bishopsford Road Bridge (Mitcham, London), that led, only 4 days after, to instability and partial collapse of the northern arch. In Italy, we should mention the failures of the Scrivia river bridge and the bridge over Cesano river (AN) following floods on November 26th 2002 [29] and March 3th 2011 [30] and the collapse of the masonry arch bridge "Ponte Verdura" (built in 1870) in Sciacca (Sicily) on February 4th 2013 by a scour-induced rigid rotation of the pier [31]. During the January 25th 2003 Basso Molise flooding events, local scouring phenomena resulted in Trigno river bridge failure by an in-plane failure mechanism [10]. More recently, the Rubianello bridge over the Aso river, in Central Italy experienced two collapses [12]. The first one during an exceptionally strong flood in December 2013 that caused the collapse of two of the sixth pier foundations and the last one during a severe flood in March 2016 when two more spans collapsed.

A noticeable example of bridge failure under shipworm-induced settlement is the historic four-arch Deba bridge in Basque, which will be examined in detail in Sect. 3. Following the foundation pole degradation by shipworm, in July 2018, the second bridge pier on the side of Deba experienced a sudden subsistence putting the bridge at risk of collapse (Fig. 2). The present paper is not dealing with the simulation of the scouring process around the bridge piers or shipworm infestation process of the foundations piles, but with the investigation of the effects (i.e. damage pattern and collapse mechanisms) and of the

load carrying capacity evaluation of the masonry arch bridge under scour/shipworm-induced settlements.

3 Deba bridge

3.1 Brief historical framework

Despite the war of Independence and the strong opposition from the king of Spain, Ferdinando VII, the Nineteen century, in Spain, was a prosperous period for masonry bridge constructions, with a strong innovative charge. This, especially, thanks to the efforts of Agustín de Betancourt y Molina, founder and manager of the Spain's first engineering college: "the School of the Corps of Engineers". In the Gipuzkoa province, all the bridges were built according to the same rules of thumb therefore, irrespective of their dimensions, number of arches or construction details, it makes sense to speak of a single design of masonry bridges until the 21th century (Fig. 3).

Particularly, the rule of Perronet exerted a considerable influence in the design of arch masonry bridge of the age. This resulted in longer bridge spans and smaller thicknesses of the piers, with a span/thickness ratio that often exceeded 1/6. Hydraulic defense structures, were also reduced in size and extension and consisted mainly in small rostra (i.e. abutments), semicircular in shape rather than triangular. Moreover the semi-circular arches passed to the segmental arches, with a rise to span ratio near 1/10.

The Deba Bridge, also known as Deva Bridge in Basque, is a stone bridge over the Deba estuary in the City of Deba in Gipuzkoa, in the autonomous community of Basque Country (North of Spain). It connects the city of Deba with the neighboring Mutriku. The bridge, built between 1865 and 1866 and inaugurated on December 18th of 1866, is a work of great engineering value as well as one of the best preserved of the Gipuzkoa Province. Consequently, currently enjoys special protection within the Monumental Complex of the Camino de Santiago (Decree No.2 of Jan 10, 2012 [32]).

The structural design of the bridge was part of a larger-scale project of coastal motorways between San SebastiÃ¡n and Bilbao. It was submitted to and approved by the General Assembly of Gipuzkoa on July 18 1863 and was designed to include passing of carriages which do not exceed the gross weight of 1500 kg. The bridge was later closed to vehicle traffic in 2007, when the new Malzaga connection (between N-634 and GI-638) on the Vitoria-Eibar Motorway (about 1 km upstream from Deba Bridge) was opened.

Failures has been a constant and treacherous threat to the life of the Deba bridge due to the geology of the riverbed, which is favorable to landslide (especially between Arrankasi and Alkolea), doline, rockfall etc. Below we list the most significant:

– **1883**: a big doline (i.e. a natural hollow) appeared in the riverbed leaving a significant part of the foundation poles timber unprotected and causing the settlement of the first and second piers on the side of Deba (right bank). Therefore, the foundation of the bridge piers were armored with rock rip-rap in the hope of stopping the slow, but nevertheless relentless, sliding and settlement of the piers and protect them from hydraulic stresses, and further erosion (Fig. 4). This interventions had not the expected effects (Fig. 5).
– **1892**: the first pier on the side of Deba suffered again a settlement of the foundation (0.34 m on the
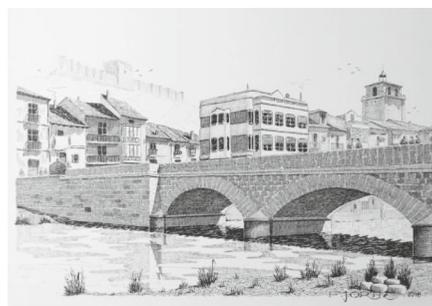
Fig. 3 Historical photos of XIX century masonry bridge in the Gipuzkoa province: **a** Deba Bridge (Gipuzkoa); **b** Leona bridge (Penafiel)
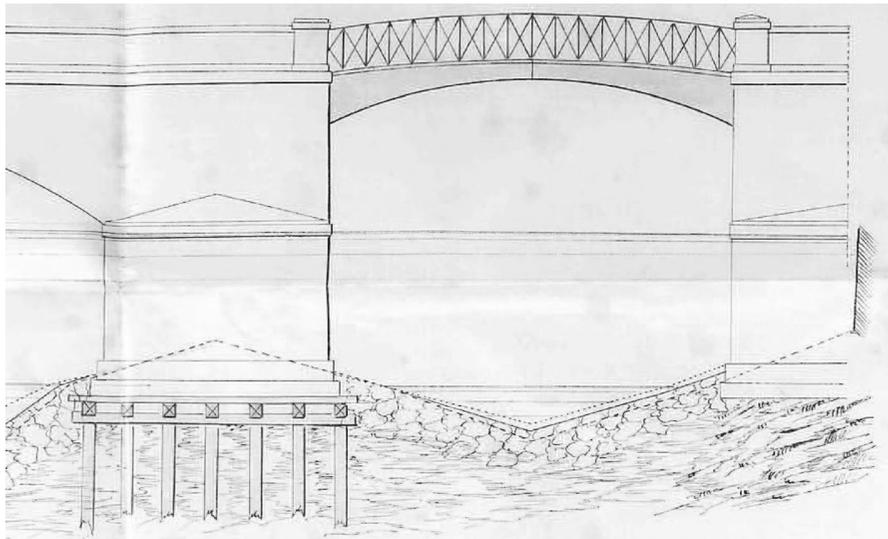
Fig. 4 Detail of the elevation drawing (from the original reparation design dated back to 1892 − 1893)
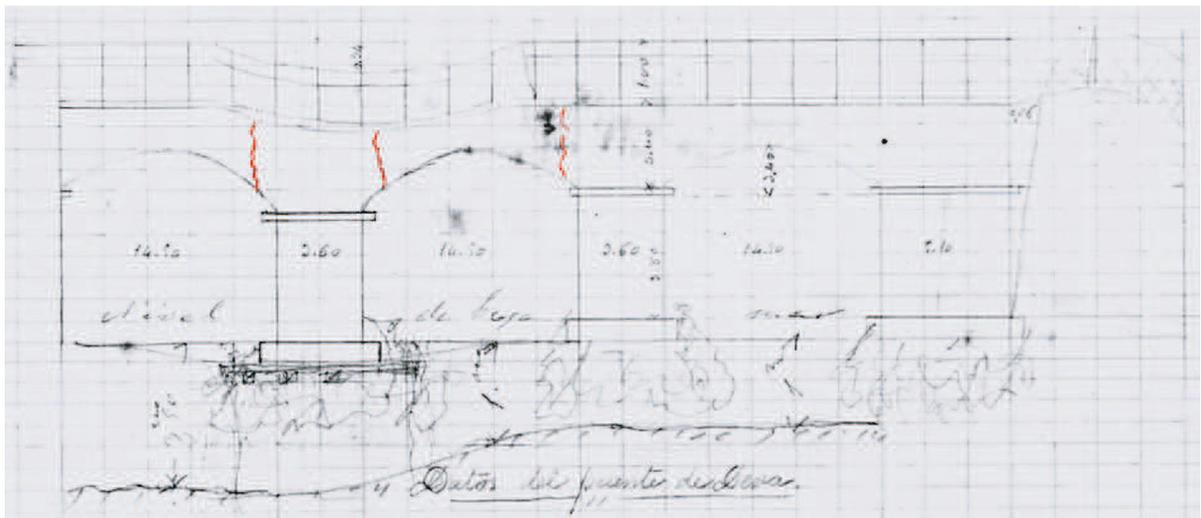

Fig. 5 A schematic representation of the 1892 bridge failure (Souce: Archivo histÃ³rico municipal-Libro de actas del Ayuntamiento de Deba: 1891 − 1895 (Signatura 65))

sea up side and $0.14\ m$ on the other side), with dislocations and damages in the bridge parapets and timpani. Inocencio Elorza examined the problem thoroughly. Under his leadership, it was decided to armor the piers foundations by exploiting the pre-existing breakwater rocks, forming a concrete base in the form of inverted vaults. These activities were articulated through a two-phase strategy. During the first phase, in 1892, maintenance activities were carried out, using about

110 m^3 of hydraulic cement and 180 m^3 of crushed stone. In the second phase, in 1893, the reparation of the bridge damages, and missing parts were performed.

– **2005**: the first pier on the side of Deba suffered a settlement of the foundation once again and then the bridge was closed to the public due to the risk of collapse.
– **2018**: the second pier on the side of Deba suffered a settlement of the foundation leading to damage of
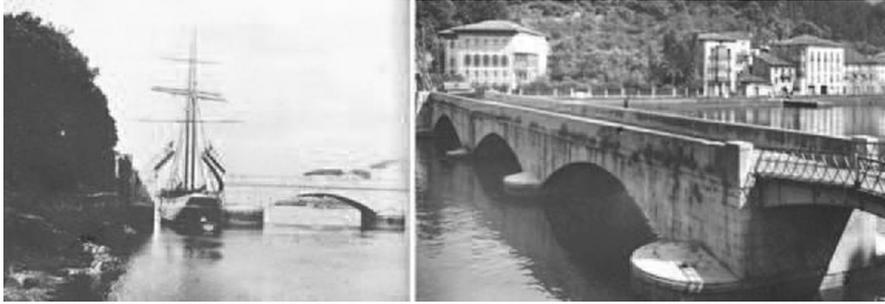
Fig. 6 Left, drawing bridge open section for the passage of the boat. Right, elevation view from the Mutriku side. Source: José MarÃ-a Izaga, Barra engineer

the two central arches, and causing failure and a pronounced twisting of the bridge deck, with the loss of parts and items. The failures were due to the degradation of the foundation's timber poles by the Xilofogo Teredo Navalis (also known as shipworm) resulting in a significantly reduction of their resistant cross section.

The last bridge restoration was performed two years before the collapse of 2018, on the occasion of the 150th anniversary of the first inauguration. However, the restoration was only limited to cleaning and maintenance operation including renovation of the street lighting and burial of exposed pipes.

3.2 Construction details

The Deba bridge is a closed-spandrel deck arch bridge with four arch spans. It is built with ashlars of local light grey limestone (i.e. bujarda-carved limestone) of excellent workmanship from the quarries of Latzur-regi, Maxpe and Milluaitz in the district of Olatz (a total of 672.45 m^3 stone masonry were used). The overall width of the bridge is 6.50 m, with one clear carriageway of 4.90 m, two sidewalks (one on each side) of 0.40 m each and two stone parapets 0.30 m wide each. Its length is 106.00 m, of which 40.90 m is the length of the approaching embankment on the right bank [33]. The embankment is made of masonry and its length represents an anomaly for the architecture of the bridges of the second half of the 19th century. The bridge parapet is also formed of grey limestone plates one meter high with a rounded edge as handrails. At the time of the failure, the bridge was made up of four segmental arches, three of them, on the East side (Deba), made of stone. They were about the same size

of 14.50 m with constant thickness of 0.80 m (i.e. 1/18 of the span), rise to span ratio about 1/6 and angle of embrace about 60°, as was into common use in masonry arch bridges of *XIX* century. The last was a reinforced concrete arch covered by a layer of stones, on the side of Mutriku (left bank). It has a span of approximately 8.70 m, constant thickness of 0.70 m, rise to span ratio about 1/6 and angle of embrace of about 70°. The concrete arch replaced an old drawing bridge, which lets boats pass upstream, to the fish markets of Maxoe and Berria (Fig. 6). It have been disposed in 1941 and dismantled in 1951 because it was no longer considered strategic.

The bridge arches rest on three equal rectangular piers and two abutments with semicircular rostra. The outer dimensions are 10.60 × 3.70 m for all piers with the only exception of the last pier on the Mutriku side that is wider, 4.80 m, to compensate the stresses that the near bank of Mutriku causes to the pier. Then, the span to width ratio for the two piers on the Deba side is about 4, that is a typical value for masonry bridges of *XIX* century. The piers rest on timber poles with maximum length of 5.00 m and average diameter of 0.30 m. They are hammered into the soil with a pitch of about 0.40 ÷ 0.6 m. Fig. 7 reports detail drawings of elevation, plan and sections of the bridge before the 2018 failure. They are extrapolated from the data and original drawings provided by the FHECOR engineer Isabel Lorenzo Pérez.

The foundations of the Deba bridge on the east side (Deba) lie in muddy ground mixed with sand and gravel and are made with 117 oak poles on which lays a large wooden raft that holds together the stone blocks foundations. Each pole is five meters long and at least twenty centimeters in average diameter. They were driven to refusal and their heads has been cut off in the
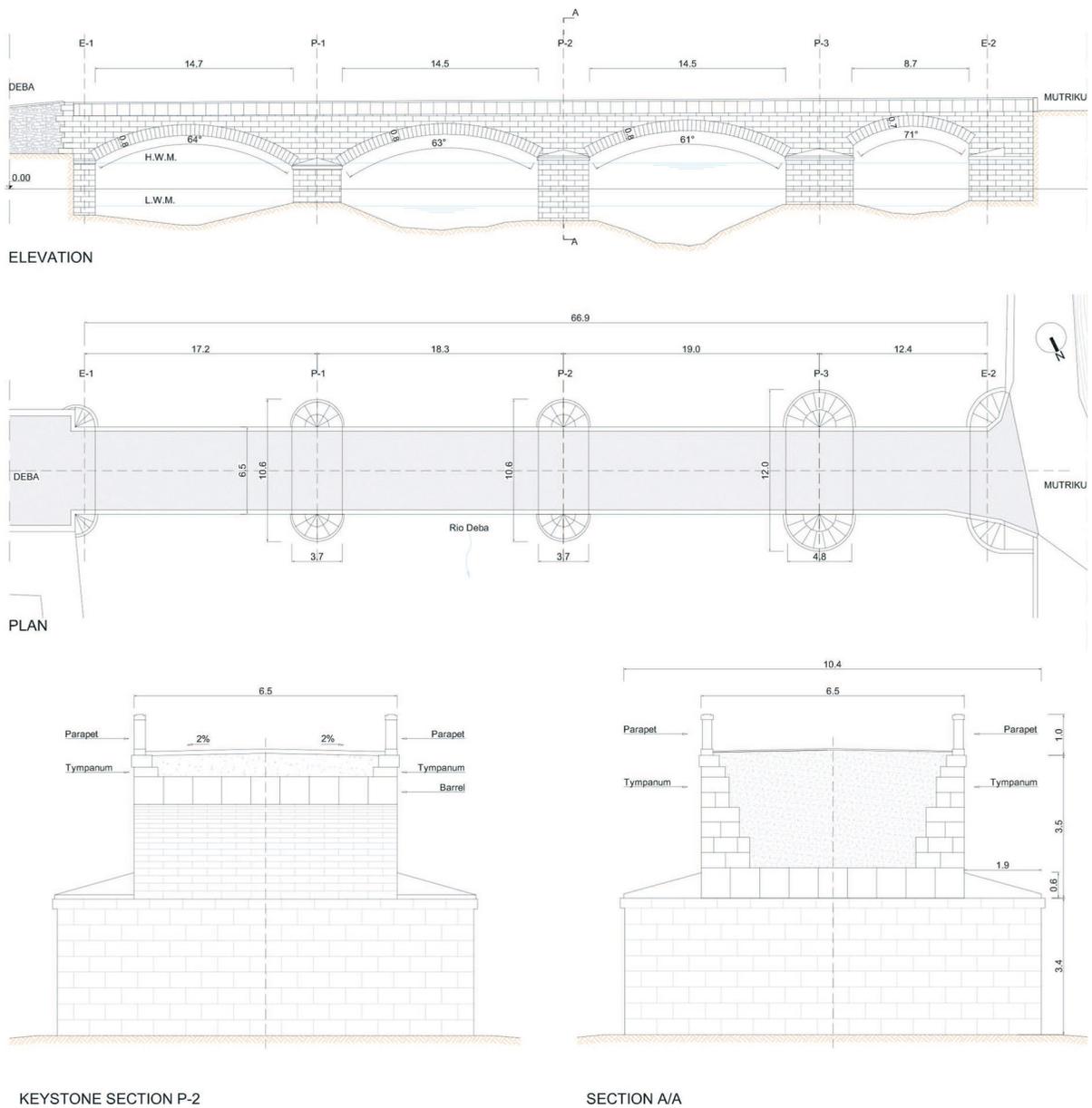
Fig. 7 Elevation, Plan and Sections of Deba Bridge before the 2018 failure. Modified from an original drawing by FHECOR Ingenieros Consultores, www.fhecor.com

same horizontal plane, about twenty centimeters from the shallow waters. Details and a schematic representation of these foundations are depicted in Fig. 8. The West abutment (Mutriku side), instead, rests directly on the rock called "Bruya".

The subsoil is composed of sandstone grey rock whose depth varies from 23 meters at the third pier closest to the Mutriku bank end to 41.40 meters in the

pier nearest to the Deba bank. The alluvial soil is mixed with different depths of silt, sand and gravel and presents strong discontinuities, particularly in the reinforced jet-grouting piers.

Finally, the bridge is supposed to have hard fill almost up to the top of the vaults, but no information could be gathered on that.
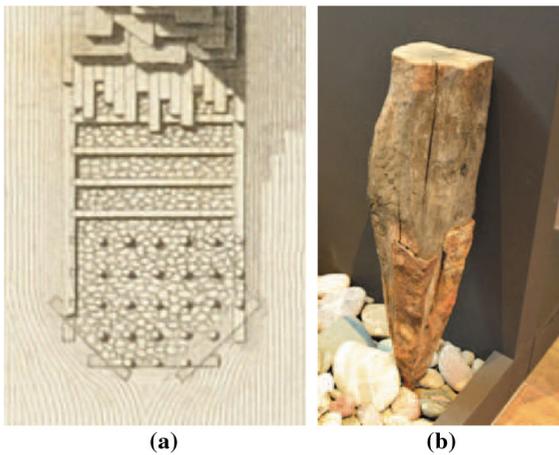
Fig. 8 Simple schematic representation of foundation. **a** A typical example of foundations with piles and wooden pile caps (from Wiebeking and Perronet); **b** lower end of a pile (Museum für Geschichte. Basel, Switzerland)

For more detailed information regarding the history and the structural details of the original structure see references by Patxi Aldaboaldetrecu [34] and Nú°ñez Julio [33].

3.3 Case study: recent Deba Bridge failure

On Thursday, July 5, 2018, at a quarter past five in the morning, and without previously observing any movement of the bridge (Fig. 9), the Deba bridge experienced a vertical settlement of the central pier (P-2). The mean settlement of the pile was about 0.80 *m*, the downstream side descending a little more. These deformations caused damage, mainly to the two central vaults (vaults 2 and 3), whose supports on pile 2 suffered displacements, torsions, loss of pieces and cracks. So there was a rotation of pier P-2 in the plane of to the bridge but no transversal rotation was observed. A great depression in the road and loss of part of the parapet downstream also appeared.

4 Numerical models

The present paper presents two different types of analysis to investigate the collapse of Deba bridge: a block-based limit analysis approach (Sect. 4.1) and an incremental-iterative FEM based approach. The modeling strategies of the two approaches are different. In the former case, we propose a block-by-block

modeling of the structure, qualitatively resembling the actual texture of the bridge. Simply put, we model the structure as an assembly of Normal Rigid No-Tension material (NRNT) blocks linked together by joints elements which comply with Heyman's assumptions (i.e. the no-tension and no-sliding assumptions). With the second approach, by contrast, masonry is assumed as a homogenized medium with elastic-perfectly plastic behaviour. Constitutive laws for the continuous media are derived from the real microstructure via the homogenization theory of periodic media. The main aims of this two-fold analysis are to compare the two approaches to each other, pointing out their own key advantages and drawbacks and proposing a refined approach that combines their advantages.

4.1 Piecewise rigid displacement (PRD) method

This section briefly outlines the Piecewise Rigid Displacement approach (PRD) for masonry. This approach falls within the so-called block-based limit analysis methods and was extensively employed in the recent literature [35–38] for its effectiveness and reliability in assessing the stability of masonry structures.

Let us consider a body composed of Normal Rigid No-Tension materials (NRNT) [2], that occupy, in a fixed reference configuration, a domain Ω of $\Re^2$, with Lipschitz boundary $\partial\Omega = \partial\Omega_N \cup \partial\Omega_D$, subjected to body forces **b** and surface traction forces **p** on the part $\partial\Omega_N$ of the boundary where the Neumann conditions are defined; and to displacements $\bar{\mathbf{u}}$ on the complementary, constrained part of the boundary $\partial\Omega_D$ (i.e. the boundary partition defined by Dirichelet conditions). For NRNT materials, and under the small strain hypothesis, the stress tensor **T** and the total infinitesimal strain tensor **E** on Ω are negative and positive semi-definite, respectively

$$\mathbf{T} \in Sym^-, \tag{1}$$

$$\mathbf{E} \in Sym^+. \tag{2}$$

Moreover, the work done by the stress tensor for the corresponding strain is zero:

$$\mathbf{T} \cdot \mathbf{E} = 0 \tag{3}$$

Fig. 9 A picture taken on May 01th 2018. On the date of the photo, there were no warning crack pattern

Restrictions (2) and (3) correspond to a normality rule of the total strain to the field of admissible stress tensors, that is a necessary condition for the applicability of the lower- and upper-bound Limit Analysis theorems.

4.1.1 Boundary value problem (BVP)

The Boundary Value Problem (BVP) for a NRNT material consists in finding an admissible state $\{\mathbf{u}, \mathbf{T}, \mathbf{E}\}$ which satisfies the equilibrium and the given set of boundary conditions (BC):

$$\text{balance equations:} \quad div\mathbf{T} + \mathbf{b} = \mathbf{0}, \quad \text{in } \Omega \quad (4)$$

$$\text{traction BC:} \quad \mathbf{Tn} = \mathbf{p}, \quad \text{on } \partial\Omega_N \quad (5)$$

$$\text{displacement BC:} \quad \mathbf{u} = \bar{\mathbf{u}}, \quad \text{on } \partial\Omega_D \quad (6)$$

where $\mathbf{n}$ is the unit outward normal to $\partial\Omega$ and $\mathbf{u}$ the displacement field.

4.1.2 PRD method: an approximate solution of the BVP

The equilibrium problem for two-dimensional masonry-like structures made of NRNT material can be formulated by means of a variational formulation of the Boundary Value Problem (BVP) [16, 39, 40]. Merely, the solution of the BVP for NRNT material corresponds to the minimum of the Total Potential Energy functional

$$\wp(\mathbf{u}) = -\int_\Omega \mathbf{b} \cdot \mathbf{u} da - \int_{\partial\Omega_N} \mathbf{p} \cdot \mathbf{u} ds \,, \quad (7)$$

defined in the field of admissible displacements

$$\mathbb{K} = \{\mathbf{u} \in X(\Omega) \text{ s.t. } \mathbf{u} = \bar{\mathbf{u}} \text{ on } \partial\Omega_D \wedge \mathbf{E}(\mathbf{u}) \in Sym^+\}, \quad (8)$$

where $X(\Omega)$ is a properly defined function space (i.e. a Banach space).

By restricting the search of the minimum of $\wp(\mathbf{u})$ in the finite class of piecewise rigid displacements $\mathbb{K}_{PRD}^M$, with support on a proper finite partition of the whole domain $\Omega = \bigcup_1^M \Omega_i$ (where Ω_i are polygons), the minimization problem becomes linear and, by using linear programming, it is to obtain an accurate approximate solution of the minimum problem

$$\begin{aligned} \text{minimize:} \quad & \wp(\mathbf{u}) = -\mathbf{c} \cdot \mathbf{U} \,, \\ \text{subject to:} \quad & \mathbf{AU} \geq \mathbf{0} \ \wedge \ \mathbf{BU} = \mathbf{0} \,, \end{aligned} \quad (9)$$

where the vectors $\mathbf{U} \in \Re^{3M}$ and $\mathbf{c} \in \Re^{3M}$ collecting the 3M rigid-body Lagrangian parameters and the external load of each partition element Ω_i, respectively. The matrices $\mathbf{A}$ and $\mathbf{B}$ reproduce the no-tension and no-sliding Heyman's assumptions $\partial\Omega_i$ of the rigid polygons Ω_i. A tolerance in block interpenetration among blocks, in the form of given eigenstrains imposed at the block interfaces is introduced in the minimum problem (9) through a negative parameter $\mathbf{g}$; so that the no-tension constraint is rewritten as

$$\mathbf{AU} \geq -\mathbf{g}. \quad (10)$$

For a specific and exhaustive description of the PRD method, see [2, 18].

4.2 Finite element model

4.2.1 Masonry model

An elastic-perfectly plastic constitutive model for masonry is adopted where, however, anisotropy in both elastic properties and strength envelope are taken into account [19, 20]. The model is formulated in the framework of homogenization theory of periodic media, referring to a block masonry structure, consisting of a periodic pattern of elastic blocks with cohesive and frictional joints. Elastic anisotropic properties for masonry (D_1, D_2, G, v_{12} and v_{21}), are derived from the closed-form approximated expression of the elastic strain energy of the above mentioned homogenized media [19], expressed as:

$$\mathcal{W}(\mathbf{E^e}) = \frac{1}{2}\left(\frac{D_1\,(E_{11}^e)^2}{(1-v_{12}v_{21})} + \frac{D_2\,(E_{22}^e)^2}{(1-v_{12}v_{21})} \right.$$
$$\left. + \frac{2v_{12}D_2\,E_{11}^e E_{22}^e}{(1-v_{12}v_{21})} + 4G\,(E_{12}^e)^2\right) \quad (11)$$

being 1 and 2 the directions parallel to bed and head joints, respectively. The coefficients in (11) depend on the elastic properties of the blocks (λ_b, μ_b) and on the normal and shear joints stiffness (K_n, K_t), as well as on the height a and width b of the blocks, as described in [19].

The elastic domain $\mathcal{G}_T$ is defined in the context of multi-surface perfect plasticity:

$$\mathcal{G}_T = \{\, \mathbf{T} \mid f^\alpha(\mathbf{T}) := \mathbf{n}^\alpha \mathbf{T} \leq 0 \quad \forall\, \alpha \in [1,..,m]\} \quad (12)$$

where $f^\alpha(\mathbf{T}) = 0$ are m independent planes, intersecting in a non smooth way, which define the yield surface. In (12), $\mathbf{n}^\alpha := \partial f/\partial \mathbf{T}$ collects the normal to the yield surfaces. In particular, if the blocks are assumed as infinitely resistant bodies and the joints as frictional interfaces, with friction angle ϕ, the yield surface comprises $m = 4$ planes which can be written in terms of the stress components as follows:

$$f^{1-2} := \frac{2a}{b}T_{11} + tg(\phi)T_{22} \pm \left(1 + tg(\phi)\frac{2a}{b}\right)T_{12} \leq 0$$
$$f^{3-4} := T_{22} \pm 1/tg(\phi)T_{12} \leq 0 \quad (13)$$

The model has been implemented in a finite element code by formulating it in the framework of classical rate-independent plasticity. It has been integrated at each Gauss point by means of a numerical procedure based on quadratic minimization. For further details, the readers can refer to [19].

5 Numerical results

5.1 PRD numerical simulation

The Linear Programming (LP) problem related to the PRD method was here solved by the Interior Point algorithm (IPA) implemented in MathematicaÂ© (Version 12) with a CPU execution time of about $5 \div 6$ minutes (Intel Core-$i7$ at 2.7 GHz, 8 GB RAM). The imposed settlements consist of two vertical displacements under the pier P-2: $\delta_1 = 0.90\ m$ and $\delta_2 = 0.86\ m$ (or, what is the same, a pier vertical displacement $\delta_1 = 0.90\ m$ and a counter clock-wise rotation $\varphi = 1.13°$ of the base of the pier P-2). Moreover, a tolerance on the interpenetration of the blocks is considered only in the tympanum region by considering negative eigenstrains g_j of 1% of the block inner diameter. Fig. 10 reports the domain discretization used in the PRD numerical simulation and the resulting failure mechanism which is a minimizer of the potential energy. The result we obtain is in good agreement with the failure geometrical survey (Fig. 10 (bottom)). One of the main features of the PRD method is that a clear subdivision of the structure into macro-blocks can be identified. This aspect is experimentally evident in most dislocated masonry structures. In the case at hand, a rigid macro-block partition of the bridge into six macro-blocks can be detected (Fig. 11b (top)) by considering the relative kinematic between the individual rigid blocks Ω_j (j=1,...,n) and a master block Ω_M. Fig. 11b shows the plot of this relative displacement with reference to the blocks constituting the structural part of the bridge in the arches, piers and abutments:

$$\Delta U_j = U_j - U^M,\ \Delta V_j = V_j - V^M,\ \Delta\varphi_j = \varphi_j - \varphi^M, \quad (14)$$

where U_j, V_j, φ_j are the rigid-body motion parameters of the *jth* block with respect to the same pole (i.e., the origin of the fixed Cartesian reference) and U^M, V^M,
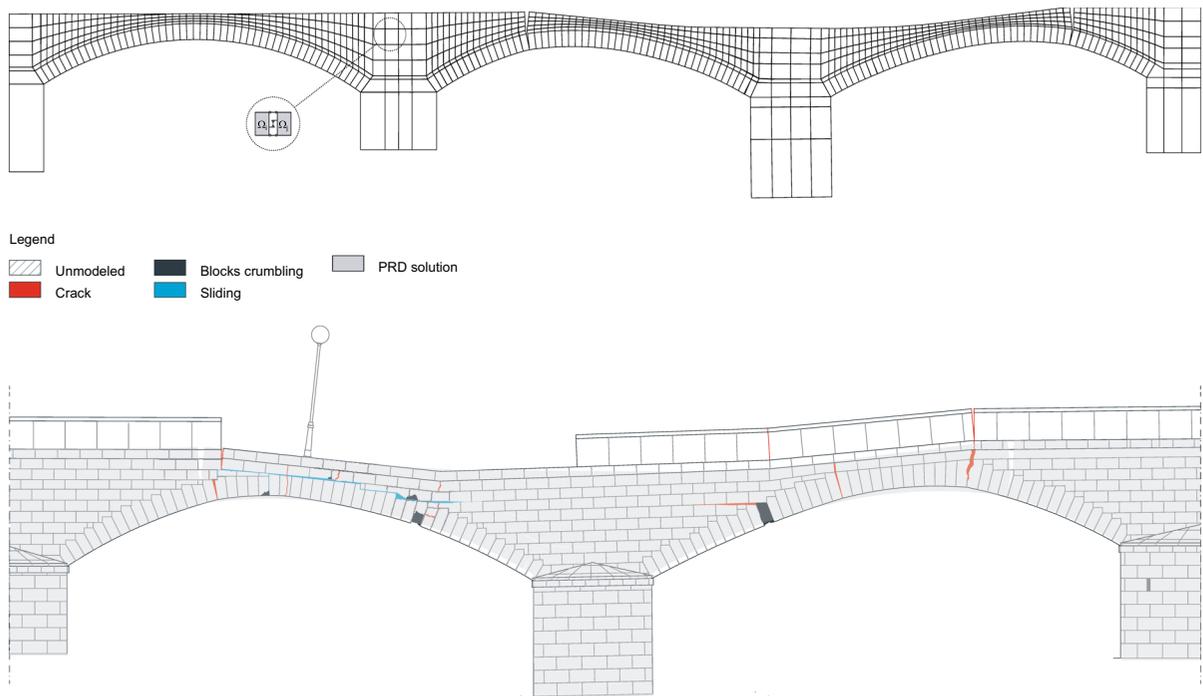
Fig. 10 PRD numerical results (top) and their superposition with the 2018 failure geometrical survey (bottom)

φ^M are the rigid-body motion parameters of the block which has been chosen as a master block Ω_M (i.e., the block located at the base of the embankment E-1). In order to allow easier visualization of the results, the relative displacements are measured on the logarithmic scale.
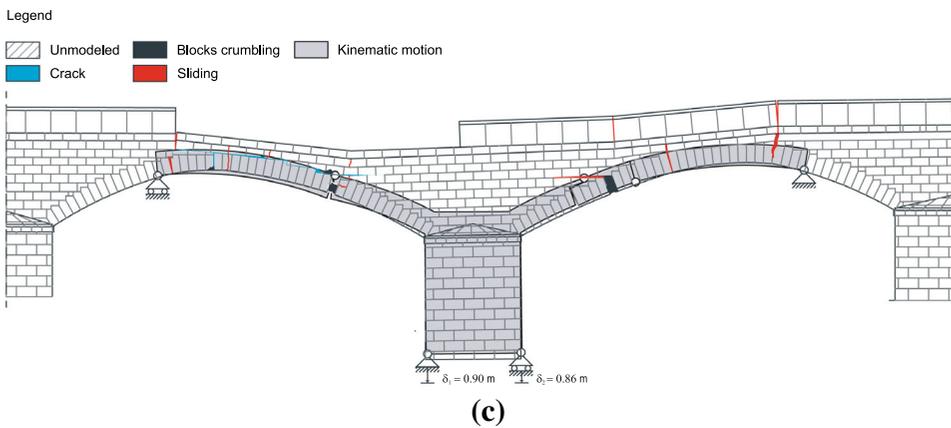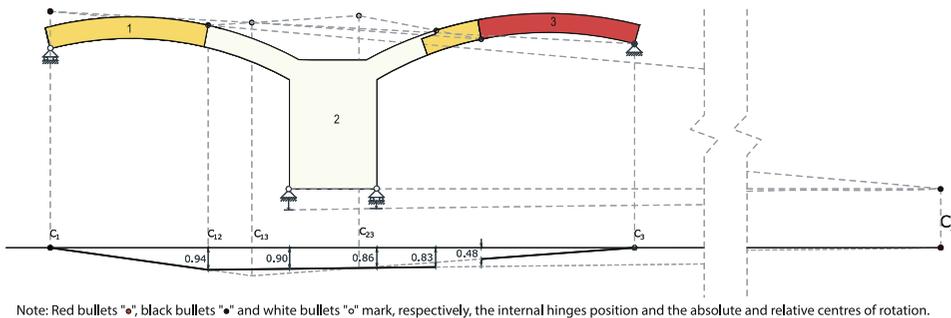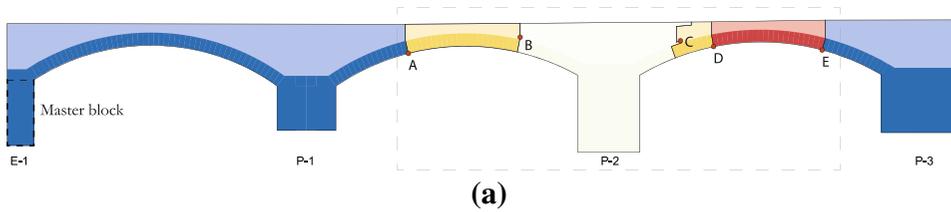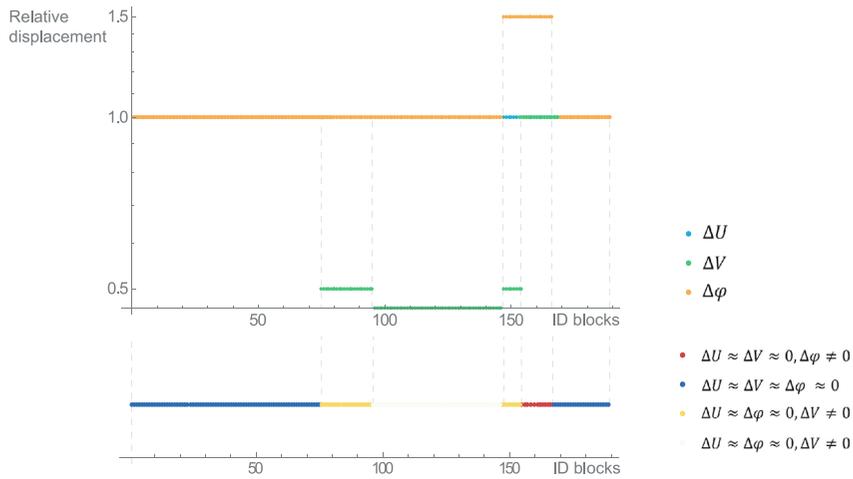
This allows to identify a cluster of about six rigid macro-blocks, hereafter marked with blue color, macro-blocks with about zero roto-translation, light and dark yellow colors, macro-blocks with non-zero vertical translation and red color, macro-blocks with non-zero rotation.

5.2 Kinematic chain analysis

In order to compare the results obtained with the PRD analysis with an elementary kinematic chain analysis, we can construct from the above described macro-block partition an elementary isostatic structure composed by four elements connected by hinges. The position of the hinges on the arches is also derived from the PRD analysis. The internal hinges between two adjacent macro-blocks (marked as *A*, *B*, *C*, *D* and *E* in Fig. 11b) are located at points belonging to common edges which exhibit zero relative

displacement in the PRD analysis. In view of the fact that the blue blocks have essentially a zero roto-traslation and that the PRD analysis allows to infer that point *E* is fixed while the point *A* translates horizontally we can assume that points *E* and *A* are both pinned, but the horizontal displacement of point *A* is free. Moreover, the points *B*, *C*, *D* can be considered as hinge joints. Finally, the isostatic sub-system shown in Fig. 11c (bottom) can be identified.

For the sake of comparison a simplified elementary geometrical kinematic chain analysis for the four block isostatic structure depicted in Fig. 11b (top) is performed. Specifically, the isostatic sub-system leads to the kinematic motion and the infinitesimal rigid body displacement depicted in Figs. 10 and 11c (bottom). The latter reveals a fairly good agreement with the results obtained with the reference method (i.e. PRD) through energy minimization. These results also are in good agreement with the failure geometrical survey (Fig. 10). Finally, it should be underlined that the relative rotations at hinges *B* and *C* produce interpenetration in the tympanum region, this is consistent both with the failure geometrical survey and with the assumption made in the PRD analysis of a

(a)

Note: Red bullets "●", black bullets "●" and white bullets "○" mark, respectively, the internal hinges position and the absolute and relative centres of rotation.

(b)

(c)

Fig. 11 a Numerical results obtained via PRD method: diagram of the relative kinematic of the blocks constituting the structural part of the bridge on a logarithmic scale (top) and resultant rigid macro-block partition of the bridge model (bottom); **b** kinematic motion of the bridge under imposed settlements; **c** superposition of kinematic motion of the bridge with the 2018 failure geometrical survey

tolerance on block compenetration in the tympanum region.

5.3 FEM numerical simulation

5.3.1 Finite element discretization

A 2D finite element model of the Deba brigde was carried out discretizing the bridge by means of triangular finite elements in plane state condition. The railing and the filling were not modeled, vertical loads simulating their weights were assumed acting on the bridge.

According to Eqs.13 the strength condition for masonry is simply defined by the dimensions of the blocks $a = 25$cm and $b = 40$cm, obtained from the geometric survey of the bridge, by the friction angle ϕ, assumed equal to $31°$ and by the orientation of the joints, according to Fig. 12. The elastic properties are defined based on the normal $K_n = 30.6$ N/mm^3 and the shear stiffness $K_t = 12.8$ N/mm^3 of the joints, and by the Young modulus $E_b = 3.18$ GPa and the Poisson's coefficient $v_b = 0.23$ of the blocks. The elastic parameters only influence the elastic branch of the global load-displacement curve (Fig. 15), but do not

influence the maximum reaction of the pier, nor the behaviour in the post-peak softening branch.

It is worth noting that, the finite element model correctly describes the stone masonry pattern, following texture orientation by assigning a proper rotation to the elementary masonry cell, as described in Fig. 12.

Two FE meshes were adopted for numerical analyses: the first one was obtained by setting a constant mesh size over the whole geometry (Fig. 13a), the second one was defined by mean of the numerical results of the PRD model (Fig. 13b). In the latter case, a mesh size equal to the previous one was adopted in the areas affected by the cracks, while a coarse mesh with double sized element was adopted in the areas where no cracks were detected. This allowed an optimization of the computational cost, limiting the number of degrees of freedom of the problem. The first mesh was composed of 2009 nodes and 3548 elements, while the optimized one was made of 1273 nodes and 2178 elements.

Numerical simulation of the settlement problem was carried out in the following way: the bridge was first analysed subjected to self-weight and vertical loads, then a maximum vertical settlement of 0.9 m with a counter clock-wise rotation of $1.13°$ was applied at the basis of P-2 pier (Fig. 7). During the settlement process, the effect of geometric nonlinearities was taken into account.

The analyses were performed with both meshes defined above. The results obtained are identical in terms of plastic strain concentration and global load-displacement curves. The average CPU time evaluated
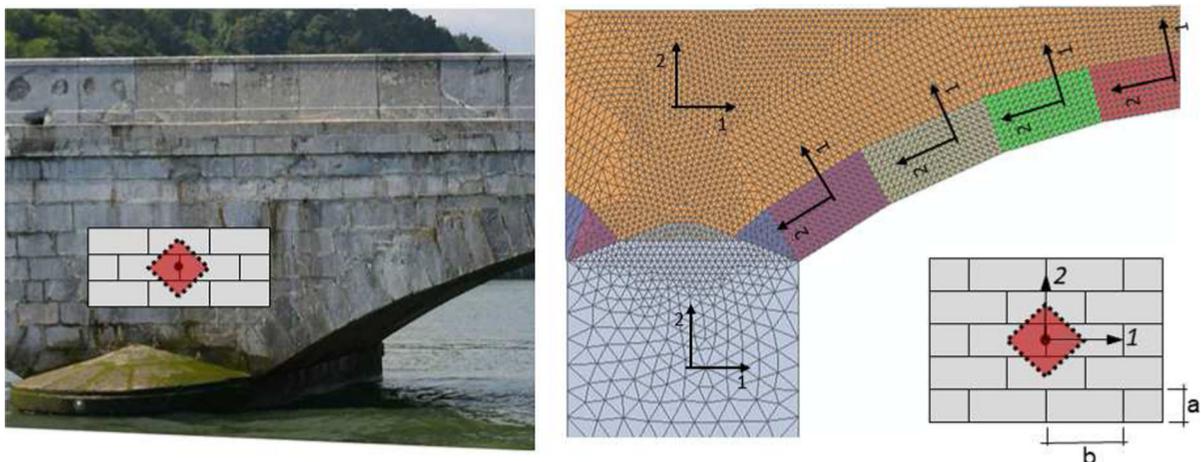

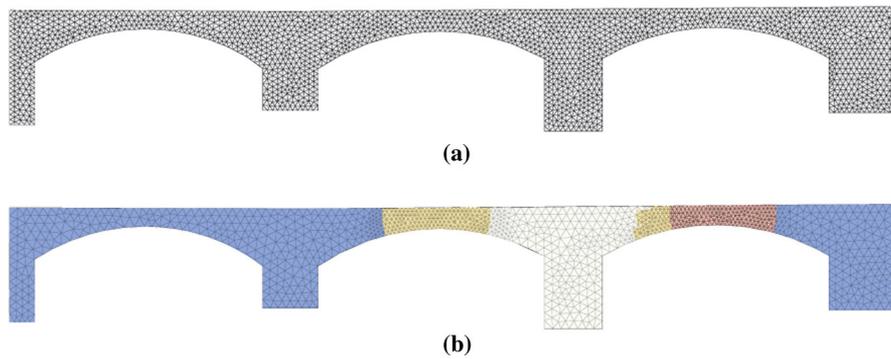**Fig. 12** Material orientations

Fig. 13 FE Mesh: fine mesh **a** and optimized mesh derived from the overlap with the rigid macro-block partition **b**

over the total number of load steps was approximately 10–11 s and 6–7 s for the first and the second mesh, respectively (Intel Core i7 at 4.0 GHz, 32.0 GB RAM).

In the follows the numerical results are referred to the only optimized mesh.

5.4 FEM numerical results

Fig.14 report the superimposition of the geometrical survey of the bridge after the settlement with the results of the FEM numerical simulation. In Fig. 14a, the concentration of the plastic strains in horizontal
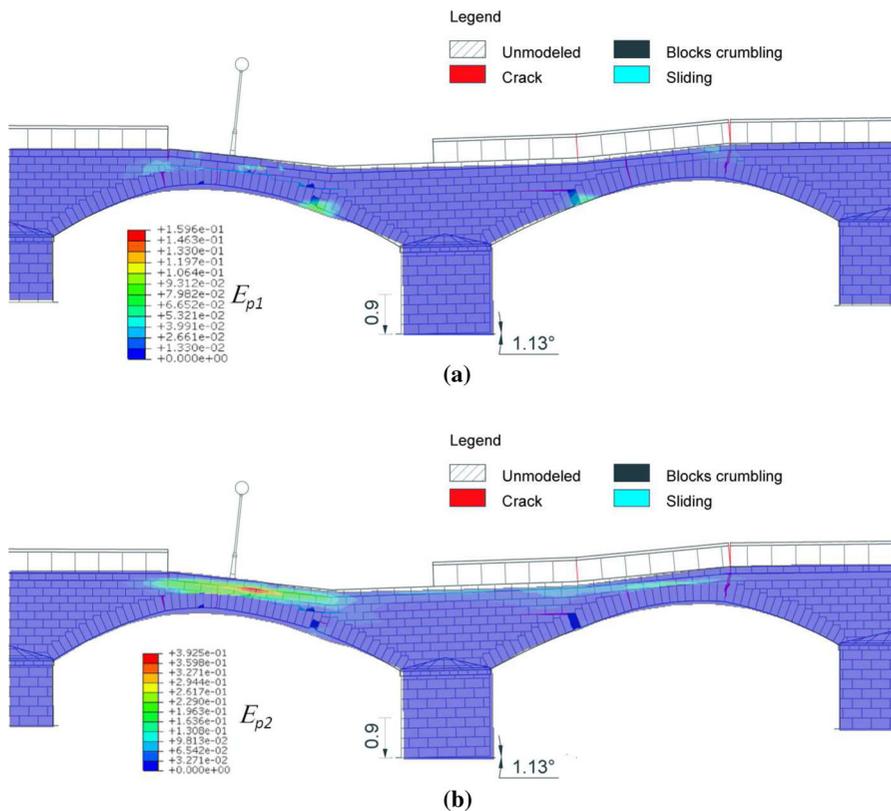
Fig. 14 Numerical result vs schematic representation of 2018 failure: **a** plastic strain concentration in horizontal direction and **b** plastic strain concentration in vertical direction
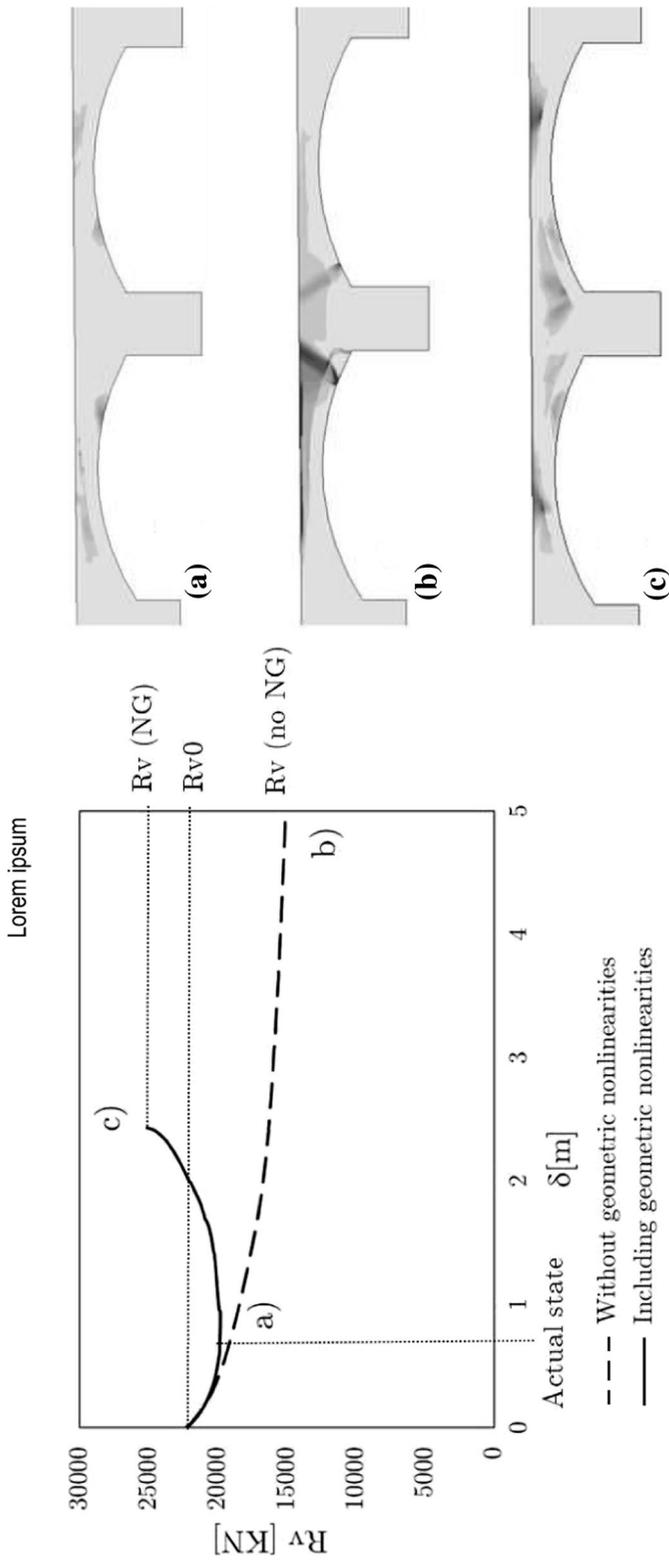
Fig. 15 Vertical reaction of the P-2 pier R_v under increasing settlement δ and corresponding inelastic deformation pattern over the bridge: **a** actual state, **b** final state under assumption of linearized kinematics and **c** final state considering geometric nonlinearities

direction are shown, while in Fig. 14b, plastic strains in vertical direction are represented.

There is a good correspondence between the numerical results and the geometric survey of the damage as shown in Fig. 14: the model is able to reproduce the development of the four hinges in the bridge and the failure of the horizontal joints in the central portion of masonry above A-2 arch.

The numerical analysis was pushed until the bridge collapsed, also taking into account the effect of geometric nonlinearities. In Fig. 15, the trend of the vertical reaction R_v at the basis of the P-2 pier versus the vertical displacement δ applied at the same pier is represented for linearized kinematics and geometric non-linearity conditions. The figure also shows the configuration of the bridge in its current state, i.e. for a vertical displacement of 0.9m, and at the end of the settling process.

In the actual state, the vertical reaction is almost the same for the two settling processes. While the two curves totally diverge for increasing displacement. More in details, the initial value before settlement R_{v0} is equal to the weight of P-2 pier plus half A-2 and A-3 spans.

During settling process, when geometric nonlinearities are not taken into account R_v decreases up to a constant value $R_v(no\ NG)$ corresponding to the self-weight of the P-2 pier plus the weight of the bridge directly supported by the pier since an arch forms that carry the weight of the two adjacent spans, as shown in Fig. 15.

If geometric nonlinearities are taken into account, the mechanism provided by the analysis at the end of the settling process, is totally different.

The same mechanism that is found in the current state persists, with a wider spread of plastic strain. The analysis also reveals that the vertical reaction has reached the minimum value in the current state and would then grow again as the settlement increases, since the displacement does not allow an upper arch to form above the pier.

It is worth noting that the maximum displacement after which the solution diverges is much lower (about 2.5 m) when taking into account geometric nonlinearities.

Finally, the same analysis was repeated for different values of friction angle ϕ in the range 24 °–35 °. The numerical results provided a variability of only

2–3%, demonstrating that the results do not depend on input parameter values.

6 Concluding remarks

A numerical tool able to predict the load carrying capacity and failure pattern of masonry arch bridges under pier's settlements is proposed. The tool is assembled by combining in sequence two different numerical models, the PRD and the FE models, that could also be used separately.

The former one does not require in input any mechanical parameter and it is based only on the geometrical configuration of the bridge. The latter essentially requires one mechanical parameter, namely the friction angle ϕ and two geometrical parameters, namely the aspect ratio of the blocks $2a/b$ and the orientation of the joints. The numerical simulations have revealed that, for this type of structure, the effect of ϕ on the results is irrelevant, and confirm the most relevant role of the geometrical configuration on the mechanical behaviour.

The two models can be adopted in sequence. The PRD model, even though able to provide alone good numerical results, gives also the possibility to optimize the finite element mesh. The finite element model gives a detailed representation of the inelastic strain caused by the bridge settlement, while also taking into account the geometric nonlinearities.

As a case-study, the settlement of one pier of the Deba bridge was analysed and the comparison with actual damage proved that both approaches are able to predict the failure pattern.

Numerical simulations of the Deba bridge under piers settlement have highlighted a relevant repair capacity of such a type of arch structures: the bridge shows a displacement capacity of about 2.5 *m* before collapse. At the same time, the careful identification of the displacement to be applied, in the present case vertical displacement plus rotation, is mandatory to catch the real failure pattern.

Furthermore, both the models do not consider a finite compressive strength, but the results highlighted that even when local crushing of masonry occurs, this is not relevant in the overall response of the structure.

Finally, the analyses have made it possible to evaluate the influence of geometric nonlinearities, which must be taken into account in order to have an

appropriate estimate of the actual displacement capacity of the structure

The proposed method stands out as a rich source of future research, for instance, in the field of the seismic assessment of masonry arch structures.

References

1. Heyman J (1966) The stone skeleton. Int J Solids Struct 2(2):249–279
2. Angelillo M (2014) Practical applications of unilateral models of masonry equilibrium. In: Angelillo M (ed) Mechanics of masonry structures. Springer, Vienna, pp 109–210
3. Cavicchi A, Gambarotta L (2005) Collapse analysis of masonry bridges taking into account arch-fill interaction. Eng Struct 27(4):605–615
4. Tubaldi E, Minga E, Macorini L, Izzuddin BA (2020) Mesoscale analysis of multi-span masonry arch bridges. Eng Struct. https://doi.org/10.1016/j.engstruct.2020.111137
5. Pelé L, Aprile A, Benedetti A (2009) Seismic assessment of masonry arch bridges. Eng Struct 31(8):1777–1788
6. Roselli I, Malena M, Mongelli M, Cavalagli N, Gioffrě M, De Canio G, de Felice G (April 2018) Health assessment and ambient vibration testing of the Ponte delle Torri of Spoleto during the 2016–2017 Central Italy seismic sequence Journal of Civil Structural Health Monitoring Volume 8, Issue 2, 1, Pages 199–216
7. Nodargi NA, Bisegna P (2020) A unifying computational approach for the lower-bound limit analysis of systems of masonry arches and buttresses. Eng Struct 221. https://doi.org/10.1016/j.engstruct.2020.110999
8. Nodargi NA, Bisegna P (2020) Thrust line analysis revisited and applied to optimization of masonry arches. Int J Mech Sci 179. https://doi.org/10.1016/j.ijmecsci.2020.105690
9. Reccia E, Milani G, Cecchi A, Tralli A (2014) Full 3D homogenization approach to investigate the behavior of masonry arch bridges: The Venice trans-lagoon railway bridge. Constr Build Mater 66(2014):567–586
10. Zampieri P, Zanini MA, Faleschini F, Hofer L, Pellegrino C (2017) Failure analysis of masonry arch bridges subject to local pier scour. Eng Fail Anal 79:371–84. https://doi.org/10.1016/J.ENGFAILANAL.2017.05.028
11. Tubaldi E, Macorini L, Izzuddin BA (2018) Three-dimensional mesoscale modelling of multi-span masonry arch bridges subjected to scour. Eng Struct 165:486–500. https://doi.org/10.1016/J.ENGSTRUCT.2018.03.031
12. Scozzese F, Ragni L, Tubaldi E, Gara F (2019) Modal properties variation and collapse assessment of masonry arch bridges under scour action. Eng Struct 199:109665. https://doi.org/10.1016/j.engstruct.2019.109665
13. Galassi S, Misseri G, Rovero L, Tempesta G (2018) Failure modes prediction of masonry voussoir arches on moving supports. Eng Struct 173:706–717
14. Tralli A, Chiozzi A, Grillanda N, Milani G (2020) Masonry structures in the presence of foundation settlements and unilateral contact problems. Int J Solids Struct 191–192:187–201
15. Anzellotti G (1985) A class of convex non-coercive functionals and masonry-like materials. Ann Inst Henri Poincaré© 2(4):261–307
16. Del Piero G (1989) Constitutive equation and compatibility of the external loads for linear elastic masonry-like materials. Meccanica 24(3):150–162
17. Giaquinta M, Giusti E (1985) Researches on the equilibrium of masonry structures. Arch Ration Mech An 88(4):359–392
18. Fortunato A, Fabbrocino F, Angelillo M, Fraternali F (2018) Limit analysis of masonry structures with free discontinuities. Meccanica 53(7):1793–1802. https://doi.org/10.1007/s11012-017-0663-8
19. de Felice G, Amorosi A, Malena M (2010) Elasto-plastic analysis of block structures through a homogenization method. Int J Numer Anal Meth Geomech 34:221–247
20. de Felice G, Malena M (2019) Failure pattern prediction in masonry. J Mech Mater Struct. https://doi.org/10.2140/jomms.2019.14.663
21. Amorosi A, Boldini D, De Felice G, Malena M (2012) Tunnelling-induced deformation on a masonry structure: A numerical approach. Proceedings of the 7th International Symposium on Geotechnical Aspects of Underground Construction in Soft Ground, Pages 353-359

22. Malena M, Portioli F, Gagliardo R, Tomaselli G, Cascini L, de Felice G (2019) Collapse mechanism analysis of historic masonry structures subjected to lateral loads: A comparison between continuous and discrete models. Comput Struct 220:14–31

23. Landolfo R, Gagliardo R, Cascini L, Portioli F, Malena M, Tomaselli G, de Felice G (2020) Rigid block and finite element analysis of settlement-induced failure mechanisms in historic masonry walls Frattura ed Integrita Strutturale. 14(51):517–533

24. Melville BW, Coleman SE (2000) Bridge scour. Water Resource, LLC, Colorado, USA

25. Richardson EV, Davis SR (2001) 'Evaluating scour at bridges', Forth Edition, Rep. FHWA-NHI 01-001, HEC No. 18, *Federal Highway Administration*, Washington, D.C

26. McIntyre F (2018) 'Tech excellence: Brougham Old Bridge repairs', *New Civil Engineer*, 14 March, pp. 50–52. See https://www.newcivilengineer.com/tech-excellence/tech-excellence-brougham-oldbridge/ 10029147.article (accessed 14/03/2018)

27. Wiggins D, Mudd K, Healey M (2019) Rehabilitation of Brougham Castle Bridge. UK, in Proceedings of the Institution of Civil Engineers - Engineering History and Heritage 172(1):7–18. https://doi.org/10.1680/jenhh.18.00027

28. Solan B, Nowroozpour A, Clopper P, Watters C, Ettema R (2019) In-situ NDT testing procedure as an integral part of failure analysis of historical masonry arch bridges, *E-proceedings of the 38th IAHR World Congress*, September 1-6, 2019, Panama City, Panama, pp. 5998–6007. https://doi.org/10.3850/38WC092019-1003

29. Torre C (2003) Ponti in muratura. Dizionario Storico-Tecnologico, *Alinea Ed.*. ISBN: 88-8125-631-2

30. Faleschini F (2018) Quality control, infrastructure management systems and their implementation in medium-size highway networks, in *TU1406 Cost Action WG4 and WG5 workshop: Sustainable Bridge Management*, 27th-28th September 2018, Barcelona, Spain

31. Bergamo O, Campione G, Donatello S, Russo G (2015) Scour-induced failure of masonry arch bridges: causes and countermeasures, in *Engineering Failure Analysis*, Vol.57, pp. 31–55. https://doi.org/10.1016/j.engfailanal.2015.07.019

32. Departamento de Medio Ambiente, Planificació³n Territorial y Vivienda (10/01/2012): 'DECRETO 2/2012, de 10 de enero, por el que se califica como Bien Cultural Calificado, con la categorÃa de Conjunto Monumental, el Camino de Santiago a su paso por la Comunidad Autónoma del PaÃs Vasco'. *BoletÃn oficial: BOPV (PaÃs Vasco)*, boletÃn 19, orden 433, disposició³n 2

33. NúÃ±ez J (1994) 'CatÃ¡logo de puentes de Gipuzkoa anteriores a 1900', PaÃs Vasco. Eusko Jaurlaritza Gobierno Vasco, Departamento de Cultura, Vitoria-Gasteiz. ISBN 8492023503

34. Aldaboaldetrecu P (2001) El Puente de Deba (Carretera a Mutriku por la costa), *Uda 2001*, Kultur Elkartea de Deba

35. Lucchesi M, Padovani C, Pasquinelli G, Zani N (2008) Masonry constructions: mechanical models and numerical applications, vol 39. Lecture Notes in Applied and Computational Mechanics. Springer, Berlin

36. Iannuzzo A, Olivieri C, Fortunato A (2019) Displacement capacity of masonry structures under horizontal actions via prd method. J Mech Mater Struct 14(5):703–718. https://doi.org/10.2140/jomms.2019.14.703

37. Iannuzzo A, Van Mele T, Block P (2020) Piecewise rigid displacement (PRD) method: A limit analysis-based approach to detect mechanisms and internal forces through two dual energy criteria. Mechanics Research Communications 107: https://doi.org/10.1016/j.mechrescom.2020.103557

38. Iannuzzo A, Dell Endice A, Van Mele T, Block P (2021) Numerical limit analysis-based modelling of masonry structures subjected to large displacements. Comput Struct. https://doi.org/10.1016/j.compstruc.2020.106372

39. Mascolo I, Gesualdo A, Olivieri C, Fortunato A (2021) On rigid blocks detection in unilateral masonry-like structures. J. of Masonry Research and Innovation, Int (in press)

40. Fortunato A, Gesualdo A, Mascolo I, Monaco M (2021) P-Bázier energy optimization for elastic solutions of masonry-like panels. Int J of Masonry Research and Innovation, (in press). https://doi.org/10.1504/IJMRI.2021.10037508